Electronic supplementary information (ESI) for

Ultrafast Sintering of Boron Nitride Nanosheet Assembled Microspheres with Strong Processability for High-Performance Thermal Management Materials

Siyuan Ding[1], Fangzheng Zhen[2,3], Yu Du[2,3], Ke Zhan[1], Yinghui Wu[2,3], Jiuyi Zhu[4], Qijun Zheng[2,3], Baofu Ding[1, 5], Aibing Yu[2,3], Minsu Liu[2,3,] Hui-Ming Cheng[1, 5], Ling Qiu[1,*]*

[1]Institute of Materials Research, Tsinghua Shenzhen International Graduate School (TSIGS), Tsinghua University, Shenzhen, Guangdong 518055, China.

[2]Monash Suzhou Research Institute (MSRI), Monash University, Suzhou 215000, China.

[3]Department of Materials Science and Engineering, Department of Chemical and Biological Engineering Monash University, VIC 3800, Australia.

[4]Institute of Process Engineering, Chinese Academy of Sciences, Beijing 100190, China.

[5]Faculty of Materials Science and Energy Engineering, Institute of Technology for Carbon Neutrality, Shenzhen Institute of Advanced Technology, Chinese Academy of Sciences, Shenzhen 518055, China

Email: minsu.liu1@monash.edu, ling.qiu@sz.tsinghua.edu.cn

This PDF file includes:

Supplementary Section S1. DEM simulation

The discrete element method (DEM) models all the particles in the whole system individually and tracks the dynamics of each particle in the system[1]. This method is based on Newton's second law and a contact model that calculates the change over time between particles. In general, a granular material is a discrete system whose physical properties are discontinuous concerning position and time. Any particle in the system can undergo translational and rotational motion described by Newton's laws of motion involving the forces and torques originating from its contact with neighboring particles and the fluid, and the resulting propagation of disturbance waves of particles and fluid far away. If the effect of interstitial fluid and non-contact forces is ignored, as is the case for the flow of coarse particles in the air, the governing equations for translational and rotational motion of particle i with mass m_i and moment of inertia I_i are given by* MERGEFORMAT :

$$m_i \frac{dv_i}{dt} = \sum_j f_{ij} + m_i g \qquad \text{(1)}$$

$$I_i \frac{d\omega_i}{dt} = \sum_j m_{ij} \qquad \text{(2)}$$

where $\mathbf{v}_i$ and ω_i are, respectively, the translational and angular velocities of the particle, f_{ij} and m_{ij} are the interaction force and the torque acting on the particle exerted by particle j or a boundary, and g is the gravitational acceleration. The equations for calculating the forces and torques were detailed in our previous studies [2–4] and are not repeated here.

Here, considering the difference in surface structures of the particles, we used a different rolling friction coefficient $\mu_{r,p-p}$ to quantify the different particle interactions

resulting from the surface structure[5]. The particle parameters are summarized in **Table S1**.

We simulated the drop of particles from a cone to investigate the flow behavior of the particles and the angle of repose. The higher the angle of repose, the better the flowability. 10,000 particles were filled in a cone. The drop height from the base of the cone to the floor was set to 750 μm. The floor consists of a small cylinder with a lip 20 μm in height and 600 μm in radius. Initially, the cone is filled with particles with a stop at the base, the base stop is removed, and the particles are allowed to flow out.

Supplementary Section S2. Structure and powder-related features of Momentive PTX60

Momentive PTX 60 is widely used as an hBN agglomerate in industry and features high flowability and isotropic thermal conductivity. Here, we characterized the morphology (**Figs. S4a-b**), powder-related properties (**Fig. S4c** and **Table S1**), and rheological properties when mixed with polydimethylsiloxane (PDMS) **(Figs. S4d-e)**.

PTX60 which was produced by high-temperature sintering showed a similar spherical structure to WBM. It is also porous and there were many protruding flakes on the surface (**Fig. S4b**). **Fig. S4c** shows the powder density of PTX60 during the tapping process to the dense packing condition, where it increased from 0.301 $g \cdot cm^{-3}$ to 0.420 $g \cdot cm^{-3}$. This value was lower than that of WBM. PTX60 had a high angle of repose of 36.8° and a high Hausner Ratio of 1.40 (**Table S1**). When mixed with PDMS, it produced a strong viscosity-enhancing property. When the filler content was 50 wt%, the viscosity of the PTX60/PDMS mixture reached 1710.4 Pa·s, which is higher than mixtures with WBM and CBM. The mixture also showed a strong shear-thickening property (**Fig. S4e**). These results indicated PTX60 has a poorer particle filling ability than WBM, much less CBM.

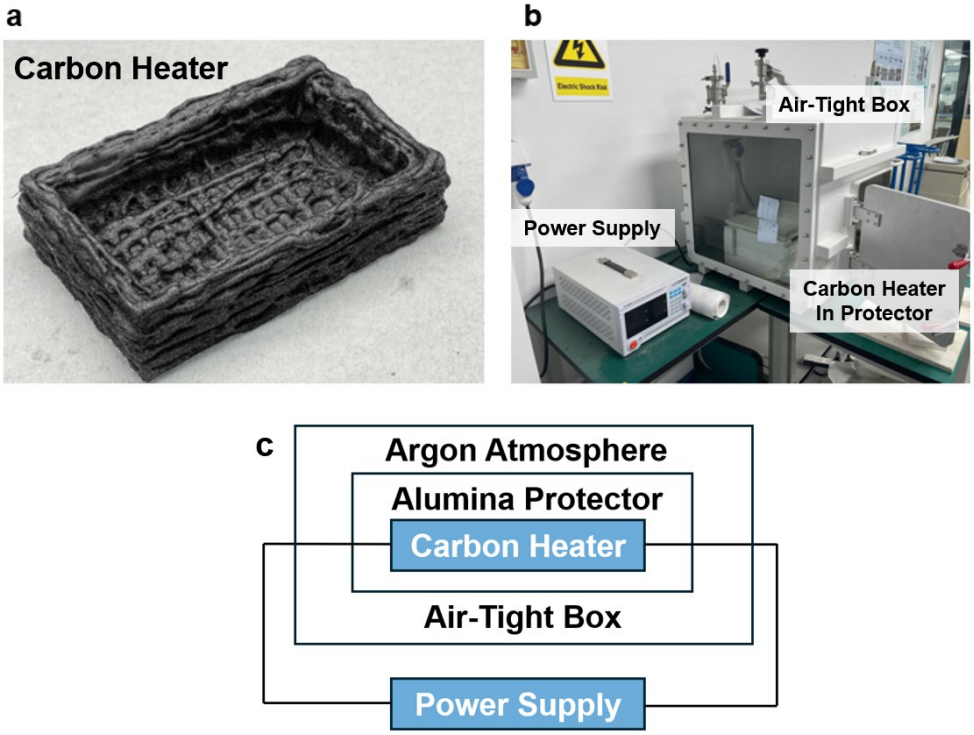

Fig. S1 Set-up of the ultrafast high-temperature equipment. (**a**) carbon heater with a size of 6 cm*4cm*2cm made by 3D printing. (**b-c**) Photo (b) and schematic (c) of the whole equipment set-up.

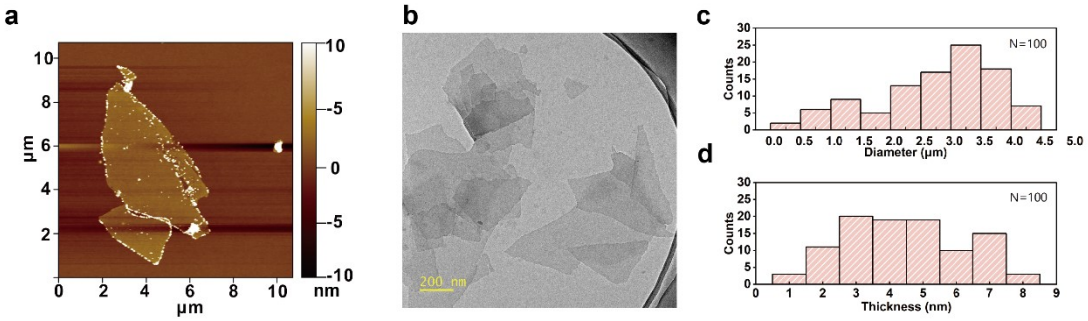

Fig. S2 Characterization of the exfoliated BNNSs. (a, b) An atomic force microscope (AEM) image (**a**) and a transmission Electron Microscope (TEM) image **(b)** of BNNS. **c, d**) Diameter (**c**) and thickness (**d**) distribution of the BNNS using AFM.

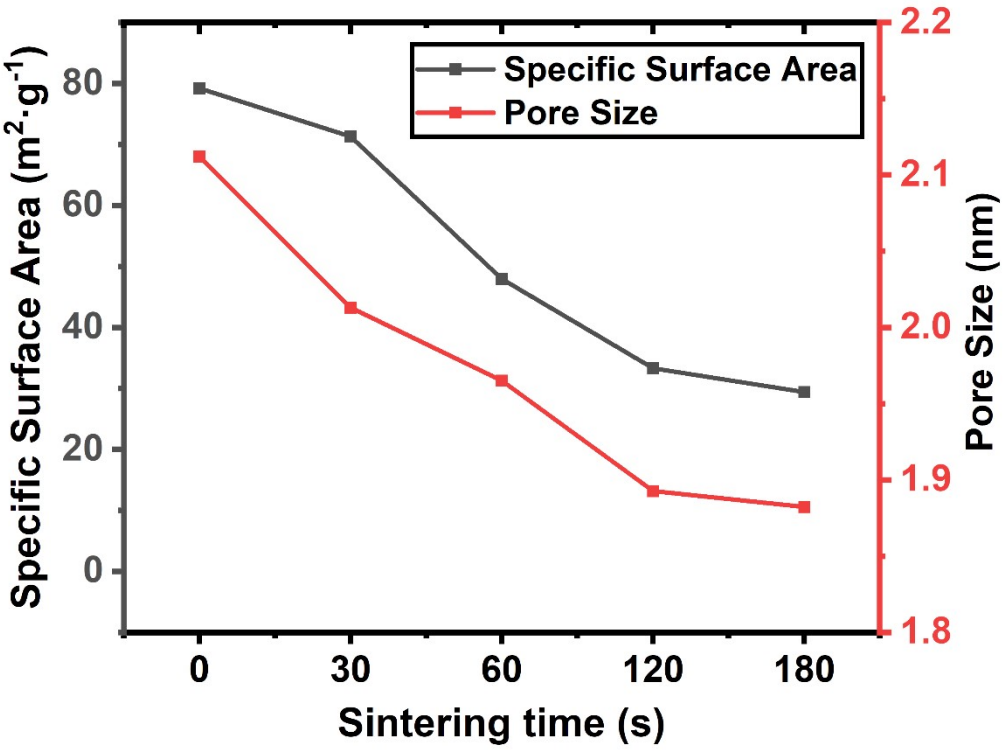

Fig. S3 Specific surface areas and pore sizes of CBMs with different sintering times.

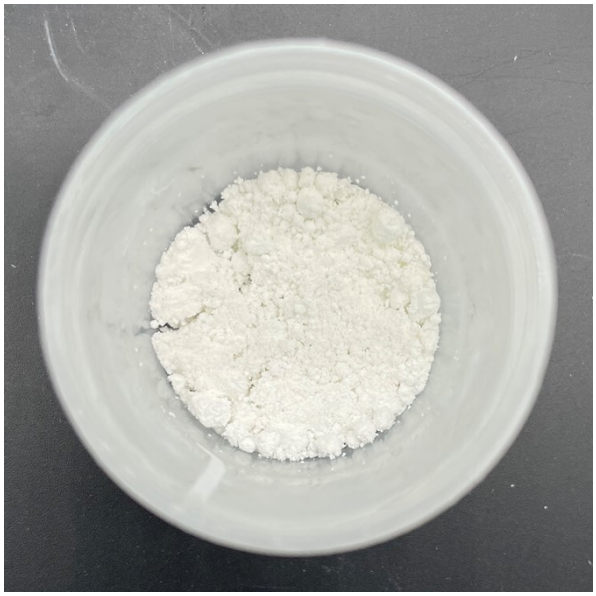

Fig. S4 Photo of the 60 wt% WBM/PDMS mixture. The mixture had a wet powder appearance rather than a paste so that the viscosity could not be tested following the same testing program.

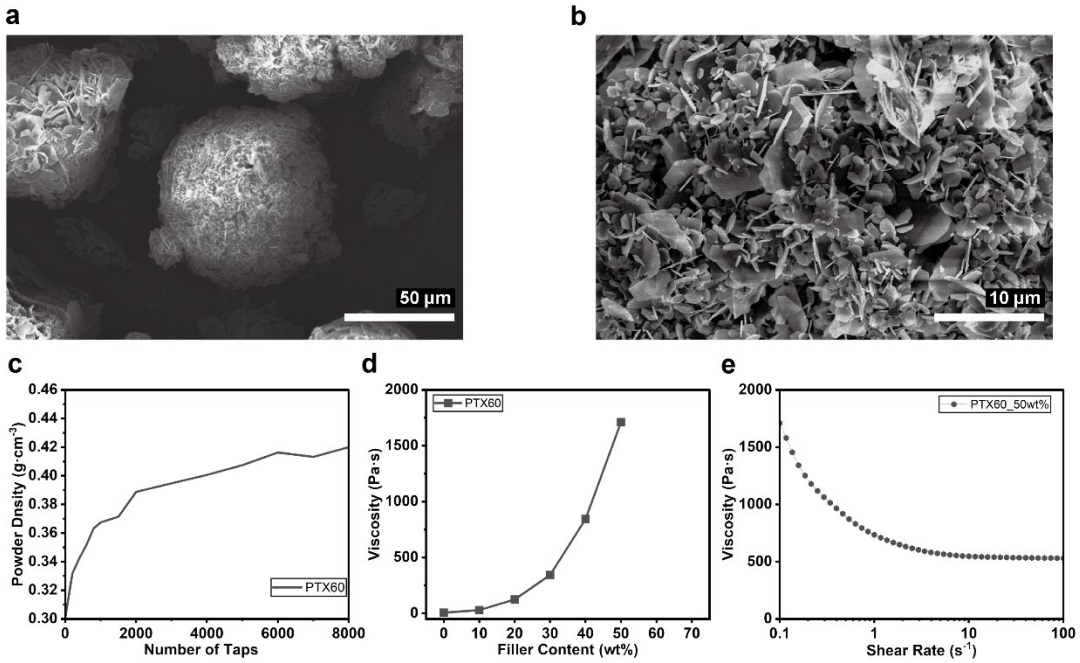

Fig. S5 Characterization of Momentive PTX60. (**a-b**) SEM images. **c**) Powder density with different tapping times. (**d**) Viscosities of mixtures with PDMS with different filler contents. (**e**) Viscosities of the PTX60/PDMS mixture under different shear rates.

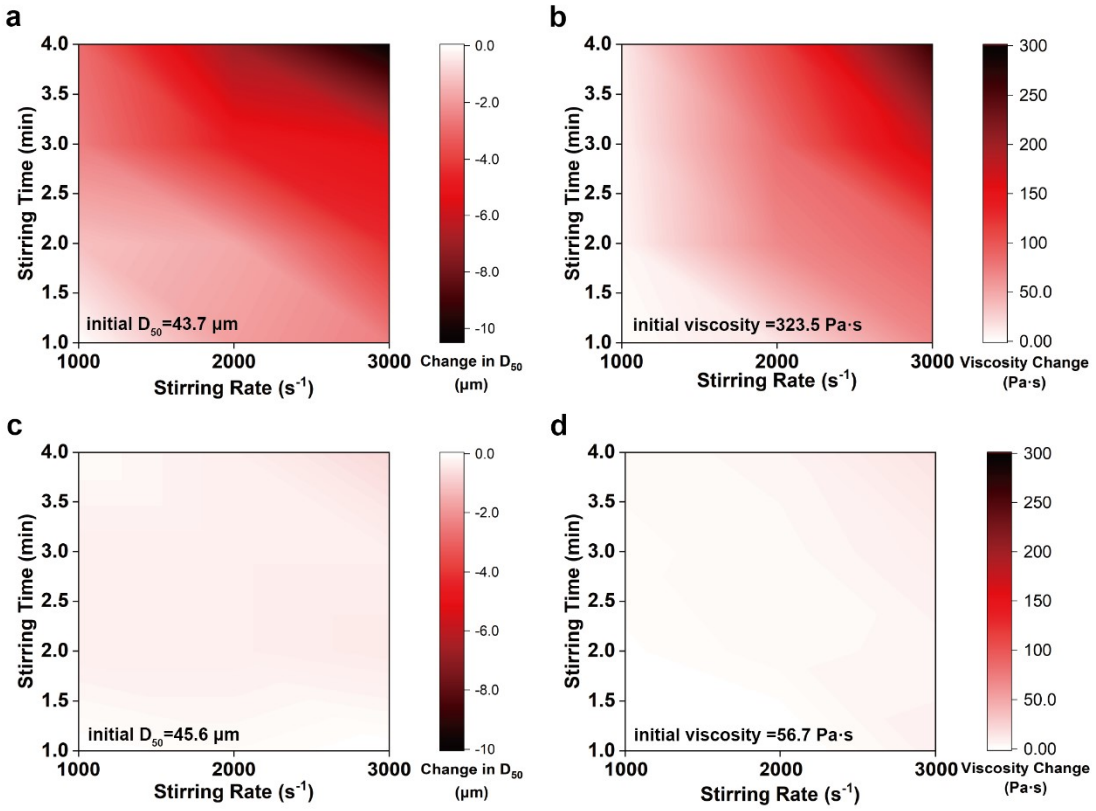

Fig. S6 (**a, b**) Change in D_{50} of WBM (**a**) and viscosity of 50 wt% WBM/PDMS (**b**) after stirring with different programs. (**c, d**) Change in D_{50} of CBM (**c**) and viscosity of 50 wt% WBM/PDMS (**d**) after stirring with different programs. The viscosities were tested with a rheometer at a shear rate of 100 s^{-1}.

Here, we used a stirring mixer to mix the particles and PDMS in the weight ratio 1:1 with different mixing programs (i.e., stirring rates and times). D_{50} was measured after washing the mixture using dimethylbenzene 5 times to remove the PDMS. When the stirring rates were higher than 1000 s^{-1}, the D_{50} of WBM significantly decreased (**Fig. S5a**) and the viscosity increased (**Fig. S5b**), indicating severe disintegration and the release of smaller particles at these stirring rates. Therefore, WBM must be processed using a lower stirring rate of 1000 s^{-1} to prevent its disintegration, and this limits the processing efficiency. A low stirring rate can also cause poor homogeneity of the mixture even with a long processing time, which could introduce pores and agglomeration in the polymer matrix and thus limit the performance[6,7]. Therefore, for WBM, a low stirring intensity is needed to avoid severe disintegration, which significantly limits the processability.

CBM, on the other hand, maintained a constant viscosity (**Fig. S5c**) and D_{50} (**Fig. S5d**) with little sign of disintegration under a variety of mixing programs, which indicated the initial structure was maintained and allowed for aggressive mixing which gave a higher processing efficiency and allowed processing freedom.

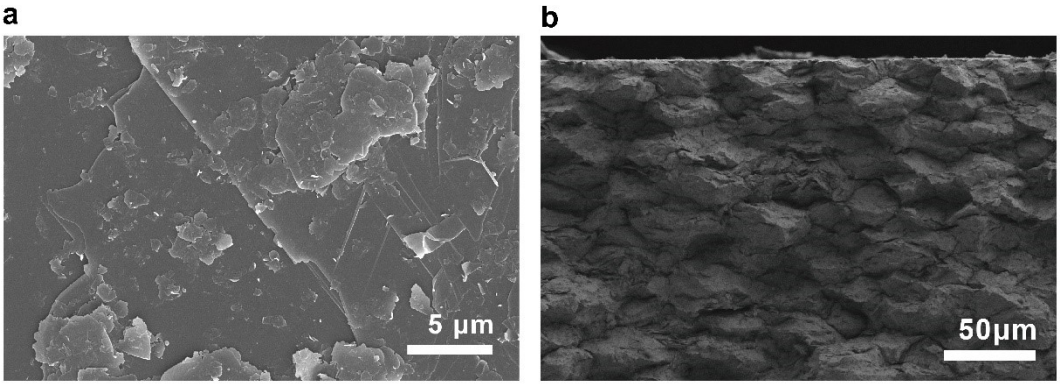

Fig. S7 SEM images of a ceramic made of CBM. (**a**) surface (**b**) cross-section.

The CBM was directly pressed into a platelet in a mold with a uniaxial pressure of 150 MPa. The platelet was placed in the UHS setup and sintered at 2000 °C for 180 seconds to achieve the product. The unsintered platelet had a density of 1.914 $g \cdot cm^{-3}$ while the sintered platelet had a density of 1.903 $g \cdot cm^{-3}$.

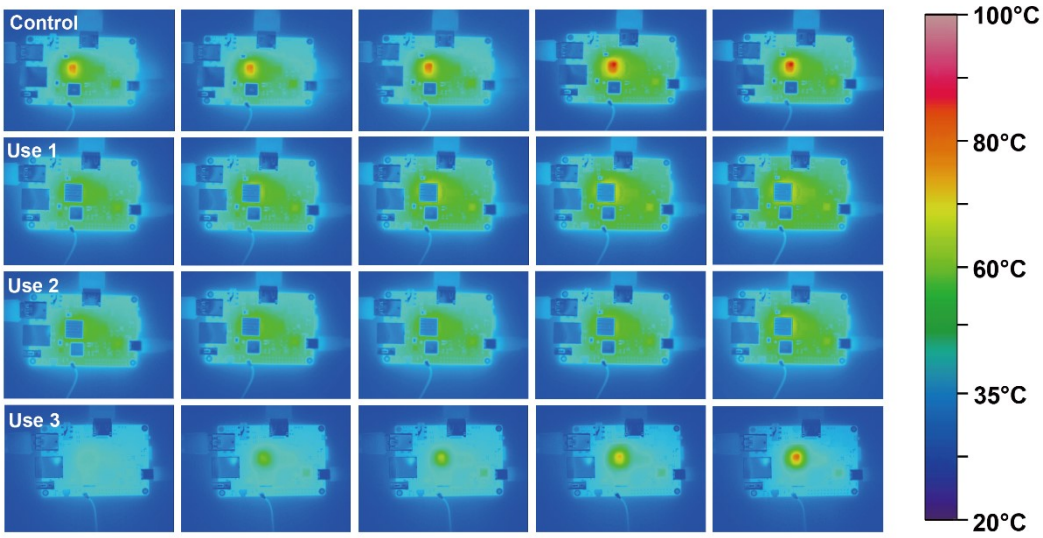

Fig. S8 Temperature distributions of the board during testing with different cooling uses.

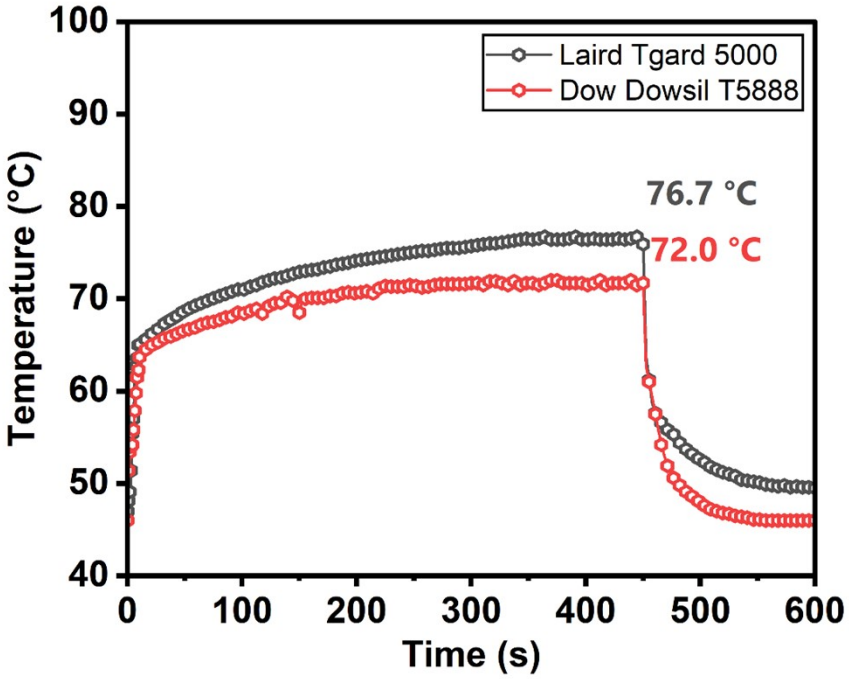

Fig. S9 Temperatures of the CPU in stress test using Laird Tgard 5000 and Dow Dowsil T5888.

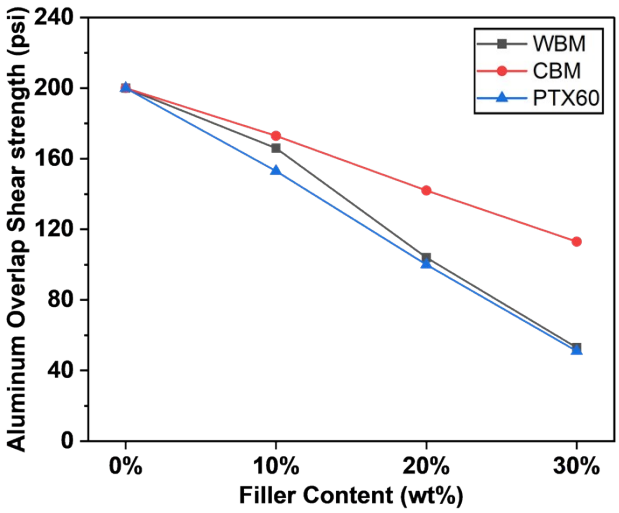

Fig. S10 Aluminum overlap shear strength of adhesives using different microspheres.

Table S1 Simulation parameters of DEM**.**

Material	Quantity	Value
WBM	Shear modulus, G_p (MPa)	5
	Poisson ratio, V_p	0.25
	Restitution coefficient, e_{p-p}	0.5
	Static friction coefficient, $\mu_{s,p-p}$	0.3
	Rolling friction coefficient, $\mu_{r,p-p}$	0.1
	Particle diameter, D_p (μm)	35, 43.7, 55, 65
CBM	Shear modulus, G_p (MPa)	5
	Poisson ratio, V_p	0.25
	Restitution coefficient, e_{p-p}	0.5
	Static friction coefficient, $\mu_{s,p-p}$	0.3
	Rolling friction coefficient, $\mu_{r,p-p}$	0.01
	Particle diameter, D_p (μm)	35, 45.6, 55, 65

Table S2 Summary of the powder properties of the Momentive PTX60.

Quantity	**Value**
Angle of repose (°)	36.8
Hausner Ratio	1.40
Apparent Density ($g \cdot cm^{-3}$)	0.301
Tap Density ($g \cdot cm^{-3}$)	0.420

Table S3 Testing data in measuring thermal conductivities of CBM and WBM.

Particle	Filler Content (%)	Thermal Diffusivity ($mm^2 \cdot s^{-1}$)	Density ($g \cdot cm^{-3}$)	Specific Heat ($J \cdot g^{-1} \cdot K^{-1}$)	Thermal Conductivity
CBM	30	0.88	1.11	1.20	1.17
	35	1.07	1.21	1.17	1.52
	40	1.55	1.26	1.19	2.32
	45	1.94	1.27	1.14	2.81
	50	2.59	1.32	1.15	3.93
	55	3.51	1.40	1.17	5.74
	60	4.75	1.45	1.16	7.99
	65	6.31	1.46	1.13	10.41
	70	6.62	1.50	1.08	10.72
WBM	30	1.00	1.02	1.21	1.23
	35	1.21	1.13	1.18	1.61
	40	1.77	1.15	1.19	2.42
	45	2.14	1.13	1.16	2.81
	50	3.08	1.22	1.12	4.21
	55	3.10	1.13	1.12	3.92

Table S4 Electrical insulation-related properties of the 65 wt% CBM/PDMS pad and Laird Tgard5000**.**

	65 wt% CBM/PDMS pad (0.10 mm thick)	Laird Tgard5000 (0.13 mm thick)
Dielectric Strength ($kV \cdot mm^{-1}$)	67.4	31.3
Volume Resistivity ($\Omega \cdot cm$)	6.8×10^{14}	1.2×10^{12}
Dielectric Constant @5.1 GHz	3.13	3.40
Loss tangent @5.1 GHz	0.0023	0.0024

Reference

1 H. P. Zhu, Z. Y. Zhou, R. Y. Yang and A. B. Yu, *Chemical Engineering Science*, 2007, **62**, 3378–3396.

2 H. P. Zhu, Z. Y. Zhou, Q. F. Hou and A. B. Yu, *Particuology*, 2011, **9**, 342–357.

3 H. P. Zhu, A. B. Yu and Y. H. Wu, *Powder Technology*, 2006, **170**, 125–134.

4 H. P. Zhu and A. B. Yu, *J Eng Math*, 2005, **52**, 307–320.

5 C. M. Wensrich and A. Katterfeld, *Powder Technology*, 2012, **217**, 409–417.

6 D. Buslik, *Powder Technology*, 1973, **7**, 111–116.

7 V. M. Barabash, R. Sh. Abiev and N. N. Kulov, *Theor Found Chem Eng*, 2018, **52**, 473–487.